

Characterization of quaternary AlInGaN films obtained by incorporating Al into InGaN film with the RF reactive magnetron sputtering technology

Kaifan Lin¹ · Dong-Hau Kuo¹

Received: 27 January 2016 / Accepted: 2 August 2016 / Published online: 10 August 2016
© Springer Science+Business Media New York 2016

Abstract Al incorporation into the InGaN films has been successfully attained from the cermet targets under the working temperature of 200 °C and output power of 120 W by the RF sputtering technique. We used energy dispersive spectroscopy to analyze the compositions of the $\text{Al}_x\text{In}_y\text{Ga}_{1-x-y}\text{N}$, and X-ray diffractometry and atomic force microscopy had been taken to obtain the crystal structure and growth characteristics of the AlInGaN films. Composition-affected electrical properties of the films had been discussed by the Hall measurement, which also identified the incorporation of Al into the InGaN film in this work. A simple n-AlInGaN/p-Si diode is designed to illustrate the potential application of the sputtered AlInGaN in an electrical device.

1 Introduction

As the III-N ternary alloys own impressive performance, they have been applied in many optical and electronic devices [1–4], and their physical and device knowledge has been well studied [5, 6]. However, regarding as one of the most promising candidates to replace the AlGaIn or InGaIn ternary alloys, the AlInGaN quaternary system has attracted researcher's attention due to its adjustable lattice parameter and wide optical bandgap range, which could be dependently determined by the composition of aluminum, gallium, or indium in the alloy. After the polycrystalline

AlInGaN alloy was firstly deposited by metal–organic chemical vapor deposition (MOCVD) technique [7], the high-quality quaternary alloy with band edge emission was attained in 1996 [8]. MOCVD has guided the III-N research directions since two decades ago. By grown on GaN/sapphire substrate with MOCVD technique, the optical property of the quaternary alloy behaved the best when the Al/In ratio is about 4.8, as the lattice constants of the alloy match that of GaN buffer [9–11]. There were many works on searching for a suitable process condition to gain alloys with higher crystallinity by adjusting the precursor inflow rate to realize the excellent solid solution [12–14]. However, the growth of AlInGaN alloy with a full range of the Al/In ratio by MOCVD had run into a dilemma due to the difficulty in having a higher Al content at higher growth temperature without the indium loss. Hence, plasma-excited molecular beam epitaxy as another possible process technique was attempted to deposit AlInGaN quaternary layers, though the results showed the limited enhancement of In content in the alloy [15, 16]. As the growth of AlInGaN is being developing, its application for optoelectronic devices is also ongoing [4].

In recent years, the quaternary AlInGaN alloy has been studied in the light emission diode (LED) area and proved to be beneficial for the performance of the device. Thin AlInGaN film was inserted into GaN barriers in the form of GaN/InAlGaIn/GaN as a multi-layer barrier of InGaIn/GaN-based LED to investigate the reduction of electron overflow and improvement in crystal quality of MQMs in the LED [17]. Meanwhile, many researchers devoted to the performance of the multiple quantum wells with AlInGaN barriers to illustrate how the compositional fluctuation of the AlInGaN layers affected on the optical characteristics of the device [17–19]. Nevertheless, no matter the MOCVD- or MBE-deposited AlInGaN films, the

✉ Dong-Hau Kuo
dhkuo@mail.ntust.edu.tw

¹ Department of Materials Science and Engineering, National Taiwan University of Science and Technology, Taipei 10607, Taiwan

quaternary film has to be grown on the expensive sapphire substrate. Even more, as the mainstream procedure for the AlInGaN growth, the MOCVD process utilizes the toxic metal–organic precursors for the formation of a high-quality film. Regardless of the attendant by-products from the MOCVD process, the unreactive precursors could be an extreme challenge for the environment-friendly industry. Furthermore, the high deposition temperature is required for AlInGaN grown with the MOCVD procedure, which may limit the further enhancement of the indium content in the AlInGaN film. Hence, the attempts for an accessible process to gain the low deposition temperature and common substrate for AlInGaN film richer in the In content have been imperatively undertaken.

With the realization of full-color InGaN LEDs fabricated on an amorphous substrate by pulsed sputtering deposition [20], the sputtering technique is inspired to be an available resolution for large-area and low-cost LEDs. For further avoiding the restriction from these small diameters and expensive wafer, numerous studies have endeavored to deposit the III-nitrides on affordable substrates instead of high-cost sapphire or SiC wafer [21, 22]. In our group, the works on the development of GaN thin film sputtered on Si substrate have been achieved [23], and the sputtered $\text{In}_x\text{Ga}_{1-x}\text{N}$ films obtained from single cermet targets showed wurtzite structure with good crystallinity [24]. For the further application, we developed all-sputtered GaN [25] and InGaN-based p–n junction [26, 27] to investigate the performance of the III-Nitrides for electronic devices. In this study, for the formation of the quaternary AlInGaN film, aluminum is attempted to incorporate into the InGaN thin film by radio frequency (RF) magnetron sputtering technology. After hot pressing a powder mixture of metallic Al, In, Ga, and ceramic GaN powders, the target for sputtering the AlInGaN film on the Si substrate is prepared. As the difficulty in having Al and In simultaneously incorporated into MOCVD-GaN, the study on sputtered AlInGaN films are filled with challenges. The microstructure, crystal structure, composition, and optical and electrical properties of sputtered AlInGaN films in this work are fully characterized and a simple p–n junction device formed by AlInGaN and p-type Si layers is designed to illustrate the rectifying I–V current.

2 Experimental detail

Three targets composed different metal and ceramic compositions were prepared to investigate the characterization of the sputtered AlInGaN films in this study. The three targets containing various aluminum compositions with the formula as $\text{Al}_x\text{In}_{0.25}\text{Ga}_{0.75-x}\text{N}$ at $x = 0.05, 0.075$ and 0.15 were regarded as target A, B, and C, respectively. The Si

(100) substrates were sliced into 1×1 cm square and washed in the acetone, alcohol, and deionized water under ultrasonic vibration scrubber 10 min for each. Three cermet targets containing aluminum, indium, gallium, and GaN powder, as shown in Table 1, were prepared by vacuum hot pressing at 375 °C for 30 min in the argon atmosphere. The sputter chamber was pumped firstly under the pressure of 1×10^{-5} torr. After the target is getting a discharge, it was filled with the inflow gasses of N_2 and argon at a flow rate of 5 sccm for each. All the specimens were sputtered at the deposition temperature of 200 °C under the pressure of 9×10^{-3} torr with RF reactive sputtering power of 120 W for 40 min. The films obtained from targets A, B, and C are abbreviated as film A, film B, and film C, respectively. A straightforward n-AlInGaN/p-Si diode was designed with Al and Pt electrodes for a n-type and p-type layers, respectively. All the electrodes with a dimension of 1×1 mm² were sputtered with their metal target at the output power of 80 W and deposition temperature of 200 °C for 20 min. The n-AlInGaN film of our n/p diode was obtained from the sputtering of $\text{Al}_{0.075}\text{In}_{0.25}\text{Ga}_{0.675}\text{N}$ target at the RF power of 120 W for 20 min. The p-type boron-doped silicon (100) with 650 μm in thickness has a smooth surface and a sheet resistance of 1–10 Ω cm.

AlInGaN films were analyzed by X-ray diffraction (XRD, D8 Discover, Bruker) to determine the quality of crystallization, and examined by scanning electron microscopy (SE-SEM, JSM-6500F, JEOL) and atomic force microscopy (AFM, Dimension, Bruker) to observe the morphology and topography. The EDS detected the compositions of the film with an attachment of the SEM with an accelerating voltage of 20 kV. Hall measurement (HSM-200, Ecopia) was used for the electrical properties of the sputtered films to obtain bulk carrier concentration, Hall mobility, and electrical conductivity. A UV–visible-NIR spectrophotometer (V-670, Jasco) was used for the optical bandgap measurement. For identifying the n-type electrical behavior of AlInGaN, a p–n junction diode was made and tested by Semiconductor Device Analyzer (Agilent, B1500A) at room temperature.

3 Results and discussion

Table 1 illustrates the aluminum, indium, gallium, and nitrogen contents of the AlInGaN films obtained from the corresponding targets A, B, and C in the formula of $\text{Al}_x\text{In}_{0.25}\text{Ga}_{0.75-x}\text{N}$ with $x = 0.05, 0.075,$ and $0.15,$ respectively. As the Al content increased and the Ga content decreased in the target, the Al content in the film slightly increased from 1.81, 2.1, to 5.23 %. Meanwhile, the Ga content remained relatively unchanged, but the In content

Table 1 Target compositions and contents (Al, In, Ga, N) in the AlInGaN thin films

Target/film	Al _x In _{0.25} Ga _{0.75-x} N target (at.%)				AlInGaN films (at.%)			
	Al	In	Ga	GaN	Al	In	Ga	N
A	5	25	7	63	1.8 ± 0.3	20.9 ± 1.6	30.6 ± 2.1	46.7 ± 3.9
B	7.5	25	6.75	60.75	2.1 ± 0.1	19.8 ± 0.3	30.0 ± 0.3	48.1 ± 0.6
C	15	25	6	54	5.2 ± 0.2	17.4 ± 0.7	28.5 ± 0.5	48.9 ± 0.7

decreased from 20.86, 19.75, to 17.42 % for the target A-, B-, and C-deposited films, respectively. The nitrogen contents were 46.73, 48.11, and 48.88 % for films from targets A, B, and C. During sputtering, the excessive metal adatoms bombarded from cermet target could be one of the reasons for nitrogen deficiency as there was no sufficient nitrogen supply for the complete nitridation reaction. While the sputtered Al-free InGaN films that reported by our group illustrated the nitrogen concentration equaled to 49.3 % [24], one of the effect of the Al incorporated into the InGaN system is conducted to weaken the sufficient nitrogen. The target A-deposited film had much lower nitrogen content, but with the Al contents' elevation, the nitrogen concentrations of the film B and C belied the amount of Al is benefit for the nitridation. On the other hand, to achieve AlInGaN films with various Al/In ratios, Yu et al. adjusted the TMIn inflow rate from 0 to 37.52 min/μmol to grow MOCVD-deposited AlInGaN film. Their result showed that the In contents of the films increase from 0 to 3.01 %, while the Al contents decrease from 13 to 7.59 % [14]. Their changes in the film concentrations of Al and In with the input fluxes go the opposite way, but it is quite consistent with our data in Table 1. It is indicated that higher In and lower Al ratios or the lower [Al]/[In] ratio in sputter target can lead to the difficulty in the nitridation of the sputtered III-nitride films. The high deposition temperature for the MOCVD procedure might be the reason to limit the further increase in the In content in AlInGaN film. Compared with the high [Al]/[In] ratio in AlInGaN films deposited by the mainstream MOCVD technique [12–14, 28], The value of In content of the MOCVD-deposited AlInGaN films is hardly greater than the one of Al content. The sputtered AlInGaN films in this study can have the lower Al and higher In contents than those made by MOCVD. As the compositional fluctuation determines the electrical and optical properties of the AlInGaN films, the sputtered AlInGaN film with a lower [Al]/[In] ratio is promising for the photoelectric devices in the future.

Figure 1 shows the HRXRD patterns of the AlInGaN films sputtered from Al_xIn_{0.25}Ga_{0.75-x}N targets at (a) x = 0.05, (b) x = 0.075, and (c) x = 0.15. From the multiple diffraction peaks and the JCPDS PDF 50-0792 as a reference, the sputtered AlInGaN films were polycrystalline in a wurtzite structure and had no second phases.

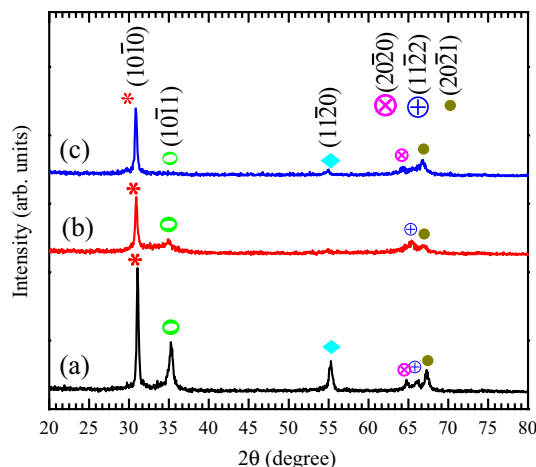


Fig. 1 HRXRD patterns of the AlInGaN films obtained from Al_xIn_{0.25}Ga_{0.75-x}N targets with a x = 0.05, b x = 0.075, and c x = 0.15

The films had a dominant diffraction peak from the non-polar *m*-(10 $\bar{1}$ 0). With the increase of the Al content and the decrease of the In content, the film showed a strongly preferred growth plane of *m*-(10 $\bar{1}$ 0). At the lower Al and higher In contents, the film deposited from the target A had random orientations in (10 $\bar{1}$ 0), (10 $\bar{1}$ 1), and (11 $\bar{2}$ 0). The random growth orientation was also observed for the sputtered In_xGa_{1-x}N films at the higher In content, while it was the preferred orientation of (10 $\bar{1}$ 0) for In-free GaN film [24]. In this work, the Al incorporation into the InGaN makes the film have a preferred growth orientation from the (10 $\bar{1}$ 0) facet, similar to the In-free GaN film. The position and the full width at half maximum (FWHM) of the dominant peak, and the lattice parameters from the three XRD data for target A-, B-, and C-deposited films are shown in Table 2. The position of the dominant peak of

Table 2 Pattern characteristic and structural parameters of the sputtered AlInGaN films from the HRXRD data

	Dominate peak		Lattice parameter		
	(10 $\bar{1}$ 0) (°)	FWHM (°)	a (Å)	c (Å)	V (Å ³)
Target A film	31.09	0.26	3.32	5.40	51.6
Target B film	30.91	0.28	3.33	5.47	52.9
Target C film	30.87	0.29	3.34	5.45	52.8

(10 $\bar{1}0$) slightly shifted to lower angle due to the small lattice expansion. Hu et al. studied the relationship between the lattice constants and the Al and In contents of the AlInGaN film. They found that the lattice parameter *c* linearly decreased with the increase of the [Al]/[In] ratio in film [29]. For our case, the [Al]/[In] ratio steadily increases for film A, film B, to film C, but the lattice parameter *c* also slightly increased, not decreased. The contradict for our data in Table 2 with the reported one is attributed to the slightly more nitrogen vacancies in the film A (Table 1) to lead to its unexpected lower lattice parameter. Therefore, the different [Al]/[In] ratios in targets have few effects on lattice parameter of AlInGaN film. Abid et al. studied the crystallinity of the molecular beam epitaxy (MBE) deposited Al_xIn_{0.1}Ga_{0.9-x}N (*x* = 0, 0.05, 0.10, 0.15, 0.20) films and found that the amount 5 % of Al incorporated into the InGaN film was significant for crystallization. With the increased Al contents, however, the crystallization of our AlInGaN films were not improved but weakened [16]. As an important indicator for crystal quality, the FWHM values of our AlInGaN films slightly increased with the increase in the Al contents of the films. The Al addition into III nitride film is not helpful for crystallization, but the In incorporation can improve the crystallinity, as had been reported for the quaternary AlInGaN films made by MOCVD [14]. Here, the Al incorporation into InGaN alloy by RF active sputtering technique is confirmed.

Figure 2a–c shows the three-dimensional (3D) AFM topographic measurements of quaternary AlInGaN films obtained from targets A, B and C, respectively. The observed surfaces had the area of 5 × 5 μm². The root-mean-square (RMS) roughness values of the AFM images were 2.17, 2.40, and 2.51 nm for the film A, B, and C, respectively. It can be seen that the roughness of the surface get coarser from the film A, B, to C. From the EDS above, the increasing [Al]/[In] ratio of the films may be related to the increase in the RMS values of the films. Compared with the RMS values of 3.78 nm of the In-free GaN film, the In_{0.25}Ga_{0.75}N and In_{0.5}Ga_{0.5}N films reduced the roughness of the films to be 1.80 and 0.45 nm, respectively. The In incorporation into GaN film is prospected to have the smoother surface and the lower RMS value [24]. Here, an increase of roughness of the AlInGaN film may be strongly related to the incorporation of the Al content to lead to a higher [Al]/[In] ratio. Thus, a hypothesis was quoted to discuss how the bombarded atoms affect the roughness of the surface during the film formation. In the comparison of InGaN and AlInGaN films deposited by MOCVD technique, Ahl et al. had mentioned that the surface mobility of Al adatom is lower than that of Ga and In adatoms, thus, Al adatom requires a longer time to diffuse uniformly after being deposited on the layer [30].

On the other words, the Al adatom may play a role in retarding the other adatoms diffusion when deposited on substrates. Yet, it's hard for aluminum to form a solid solution with gallium directly under low temperature. The indium possesses the capability of dissolving aluminum and gallium together. Therefore, the addition of indium is important to facility the Al incorporation into GaN [31]. However, the diffusions of the In and Ga atoms are expected to be interfered by the Al adatom to lead to a rougher surface. Therefore, the Al content of the films is positive to the surface roughness. On the other side, Fig. 2d–f illustrates the morphologies of the SEM images of AlInGaN films deposited from target A, B, and C, respectively. Their cross-sectional SEM images are attached at the corners of the corresponding plain-view images. Observed from the cross-sections, we can find that all the sputtered AlInGaN films have excellent adherence to the Si substrates with a thickness of about 1.1 μm. There are no cracks in films. The surfaces of the sputtered AlInGaN film are continuous, smooth, and free of pores. As the polycrystalline nature of our films, there are no V-shape pit defects, as observed from MOCVD-AlInGaN [32].

As shown in Fig. 3, the room-temperature electrical properties of the AlInGaN films obtained by target A, B, and C were plotted by the effective electron carrier concentration (*n_e*), Hall mobility (*μ*), and electrical conductivity (*σ*). All the AlInGaN films behave the n-type semiconductor with *n_e* values of 2.0 × 10¹⁸, 1.02 × 10¹⁸, and 8.67 × 10¹⁷ cm⁻³, *μ* values of 466, 523, and 1220 cm² V⁻¹ s⁻¹, and *σ* values of 156.6, 85.4, and 170.5 S cm⁻¹ for the films A, B, and C, respectively. Observed the values of electron carrier concentration from films A, B, to C, the *n_e* values decreased from 2.0 × 10¹⁸ to 8.67 × 10¹⁷ cm⁻³ with the enhancement of Al content and the reduction of In content in the films. Meanwhile, the mobility of the films increased from 466 to 1220 cm² V⁻¹ s⁻¹, and the *σ* values reached a minimum of 85.4 S cm⁻¹ for film B. To recognize the behavior of the carrier concentration in the quaternary AlInGaN system, S.F. Yu and his group controlled the growth conditions of varying the TMIn flow rate under a constant TMAI flow to grow the AlInGaN epilayers by MOCVD technique. The result showed the increasing In content accompanied by the decrease in the Al content of the AlInGaN films lead to the enhancement of the carrier concentration *n_e* from 3.47 × 10¹⁷ to 6.75 × 10¹⁷ cm⁻³ [14]. The similar behavior of *n_e* affected by In content was mentioned by C. C. Li et al., they reported the works of studying the characteristics of In_xGa_{1-x}N (*x* = 0, 0.25, and 0.50) films sputtered from single cermet targets, and the *n_e* values of the In-free GaN, In_{0.25}Ga_{0.75}N and In_{0.5}Ga_{0.5}N films were

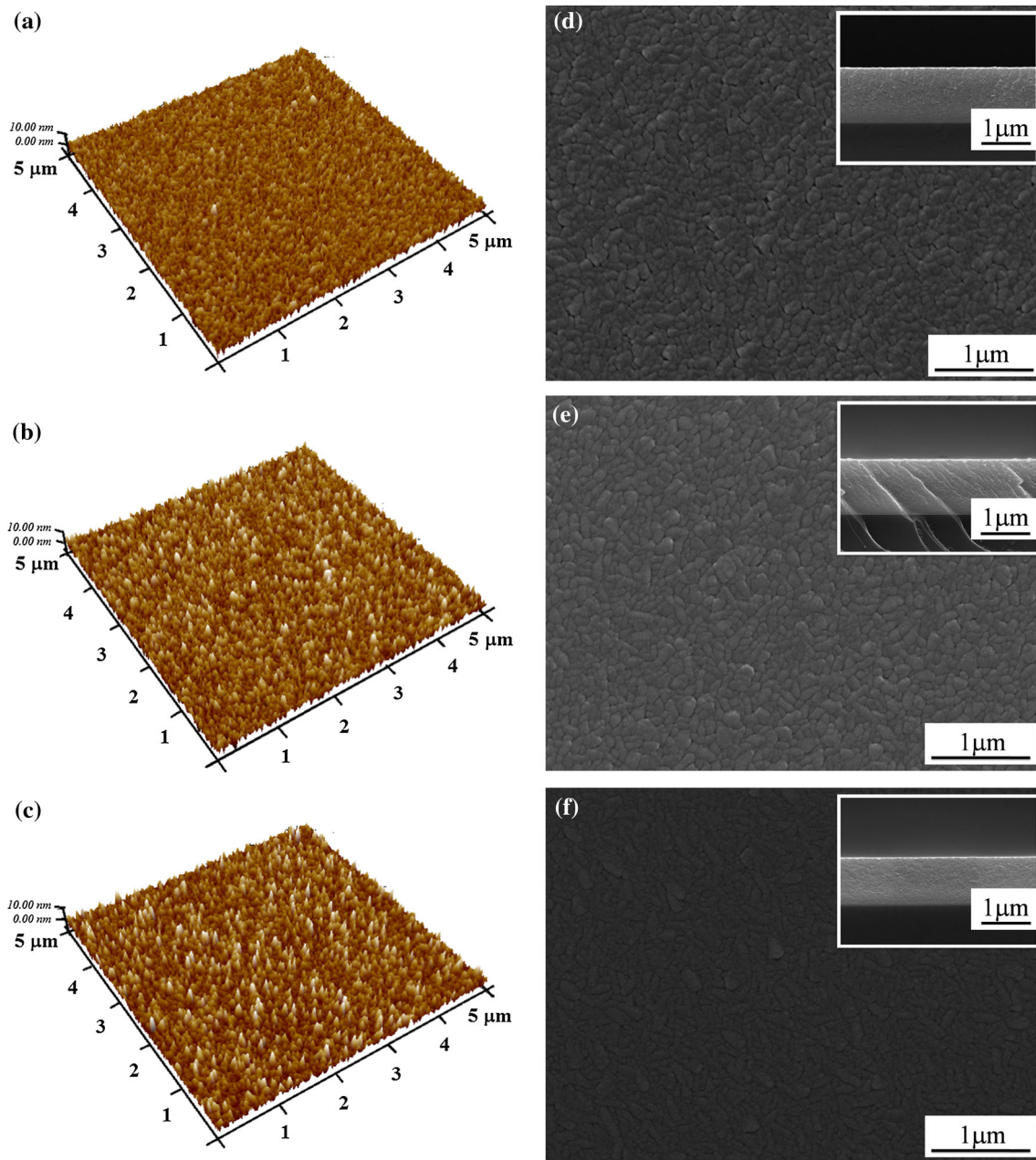


Fig. 2 AFM images (a)–(c) in $5 \times 5 \mu\text{m}^2$ and FESEM scanning images (d)–(f) of AlInGaN films obtained from $\text{Al}_x\text{In}_{0.25}\text{Ga}_{0.75-x}\text{N}$ targets for **a** and **d** $x = 0.05$, **b** and **e** $x = 0.075$, **c** and **f** $x = 0.15$. The cross-sectional views *inset* corners in corresponding SEM images

3.07×10^{18} , 1.06×10^{20} and $1.73.67 \times 10^{20} \text{ cm}^{-3}$ [24]. As is seen that the 25 % amount of indium incorporated into GaN film results in the rapid enhancement of n_e values from 3.07×10^{18} to $1.06 \times 10^{20} \text{ cm}^{-3}$, In content has shown the function to improve the electron concentration in the InGaN system. After compared with high n_e values of Al-free InGaN film, the reduction of n_e values in InGaN can be noticeable if Al is also incorporated. The trend in the changes of electrical properties is also confirmed with the work done by Liu et al. [33]. For the electrical mobility, it is higher in the InGaN system, as compared with the In-

free GaN films. Although the increase in the In content of $\text{In}_x\text{Ga}_{1-x}\text{N}$ films can enhance the mobility, the over-substituted InGaN cannot further increase its mobility due to the retardation by the high n_e value [24]. As the Al content in AlInGaN system had shown to enhance mobility, Li et al. [34] also theoretically calculated the electron mobility as a function of AlInGaN alloy composition based upon the disorder scattering in AlInGaN/GaN heterojunction. In this work, the mobility values elevated rapidly from 523 of the film B to $1220 \text{ cm}^2 \text{ V}^{-1} \text{ s}^{-1}$ of film C, as the Al contents rapidly increased from the films B to C (Table 1). Thus, the

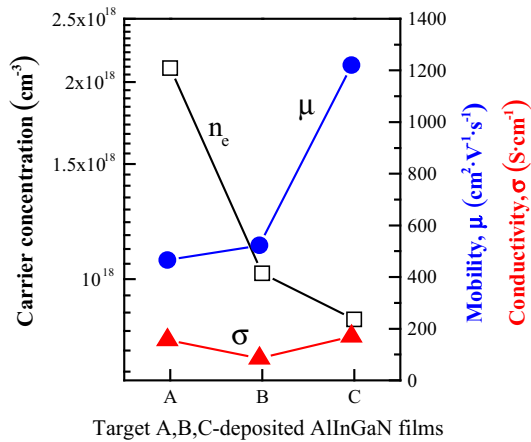


Fig. 3 Plot of electron concentration (n_e), mobility (μ) and electrical conductivity (σ) of the AlInGaN obtained by the three targets

Al incorporation in the AlInGaN system has two significant effects on the decrease in n_e and the increase in μ . On the other side, electrical conductivity is regarded as the product of electron concentration and mobility. As shown in the Fig. 3, a minimum is achieved due to the different trends of n_e and μ with the increase in the Al content.

Figure 4 shows the optical band gap of the AlInGaN films sputtered from the targets A, B and C with the Tauc plot method. The graph is plotted with photon energy ($h\nu$) along the X axis and $(\alpha h\nu)^2$ along the Y axis. The series of data gained from the UV/NIR–visible measurement, and the $(\alpha h\nu)^2$ data were transformed from the absorption coefficient of the films, which deducted the reflection or absorption losses caused by the substrates. After plotting $(\alpha h\nu)^2$ versus $h\nu$ curve, we can calculate the optical band gap by extrapolating the linear part of this $(\alpha h\nu)^2$ – $h\nu$ plot. The optical band gap was calculated by Tauc plot with an equation

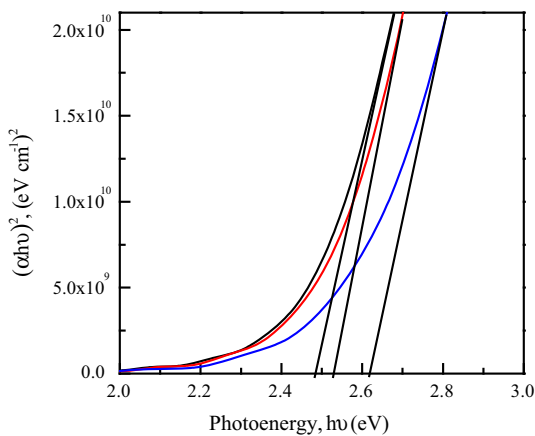


Fig. 4 Tauc plot of $(\alpha h\nu)^2$ versus photon energy of the AlInGaN films deposited by target A (left), B (middle) and C (right). The optical bandgaps are identified by extrapolation of the straight line portions to energy axis

$$(\alpha h\nu)^2 = A(h\nu - E_g) \quad (1)$$

where α is absorption coefficient, E_g is an optical bandgap of a thin film, A is a constant, and $h\nu$ is the incident photon energy. As Tauc plot contains the intrinsic defects of the accuracy due to the manual extrapolating line, the approximate values of the band gap for the films A, B, and C are 2.48, 2.53, and 2.64 eV, respectively. As the extrapolation lines are clearly plotted in Fig. 4, the optical band gap of the AlInGaN films is slightly enhances with the increase in the Al content. In our previous reports about the optical properties of Al-free InGaN films [24]. Due to the indium induced high electron concentration that confined to the bottom of the conduction band, which led to bandgaps shift to high energy region so called Brusstein–Moss shift effect, the In incorporation into the GaN films contributed to the reduced values of the bandgap. Meanwhile, the eminent decrease value of the electron concentration caused by Al incorporation into InGaN system, and it results in the bandgap of AlInGaN shifting to low energy region. The properties of the AlInGaN film are strongly determined by In and Al contents [10]. However, the mainstream MOCVD-processed AlInGaN film has been limited with the low In content and high Al content [35]. Hence, the primary studies of the AlInGaN alloy in the optical application have been focused on the ultraviolet light-emitting diodes [36–38]. In this work, the sputtered AlInGaN films obtained from a cermet target contain lower [Al]/[In] ratio and show the much adjustable band gap behavior closer to the visible light region. However, the probability and property of the sputtered AlInGaN film applied for electronic devices need to be discussed and demonstrated. Hence, a straightforward n-AlInGaN/p-Si diode is designed in this work, and the characteristics of I–V curve is illustrated below.

Figure 5a shows the schematic plot of the Al/n-AlInGaN/p-Si/Pt device and (b) illustrates the current density

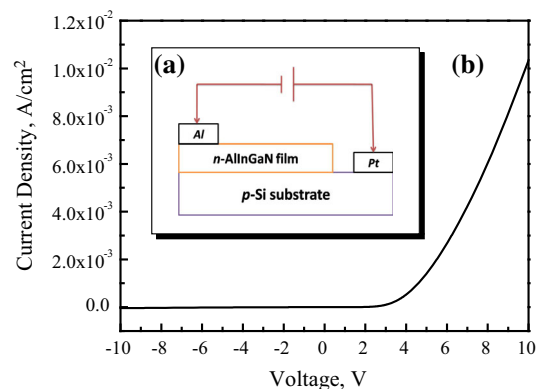


Fig. 5 a Schematic diagram of Al/n-AlInGaN/p-Si/Pt diode and b current–voltage characteristic of a p–n junction diode containing AlInGaN film obtained from $\text{Al}_{0.075}\text{In}_{0.25}\text{Ga}_{0.675}\text{N}$ target

(J)–voltage (V) characteristic of the straightforward p–n junction measured at room temperature with a one mm² contact. Here, the n-AlInGaN layer of the p–n junction in this work was sputtered from the Al_{0.075}In_{0.25}Ga_{0.675}N target. As shown in the figure, the applied voltage extended from –10 to 10 V for the current density–voltage measurement of the device. Observed from the Fig. 5b at the forward bias of 10 V, the current density of the diode was found to be 10.4 mA cm^{–2}. At the reverse voltage of –5 V, we found the leakage current density to be 1.21 × 10^{–5} A cm^{–2}, and the turn-on voltage of the straightforward diode was at 2.70 V. Few studies involving J–V characteristics of the AlInGaN films have been reported. The J–V curve plotted from CVD-grown n-Al_{0.08}In_{0.08}Ga_{0.84}N film with Pt Schottky contact, published by Alaa J. Ghazai et al., showed the diode contains the turn-on voltage below 2 V [39]. The fabricated device in this work showed the ability of blocking current even at reverse bias of –10 V. In the previous report, a similar p–n junction of n-In_xGa_{1–x}N/p-Si diodes containing In contents of x = 0, 0.15, and 0.40 was designed and showed leakage current densities of 5.96 × 10^{–5}, 8.05 × 10^{–5}, and 2.81 × 10^{–4} A cm^{–2} (at –5 V), respectively [26]. The indium incorporated into GaN was concluded to increase the leakage current values of the diodes. Compared with the data from Al-free InGaN-based device above, our aluminum-incorporated InGaN film has a reduction in the leakage current density.

Based on the standard thermionic-emission mode, the electrical characteristics as ideality factor and barrier height of diode can be evaluated by using an equation expressed as below [40] under the condition of qV > 3kT: it can be expressed as below.

$$I = I_s \exp\left[\frac{q}{nkT}(V - IR_s)\right] \tag{2}$$

where *I_s* is the saturation current, *q* the electronic charge, *n* the ideality factor, *k* the Boltzmann constant, *T* the experiment temperature in Kelvin, *V* applied voltage and *R_s* the series resistance. The series resistance *R_s* could be ignored at low saturation current and the barrier height ϕ_B could be calculated from saturation current determined by extrapolation of the curve in the plot of ln(*I*) versus *V* at *V* = 0. Here, the barrier height ϕ_B of the diode was calculated according to:

$$\phi_B = \frac{kT}{q} \ln\left(\frac{A^*AT^2}{I_s}\right) \tag{3}$$

where *A* is the diode area and *A** the effective Richardson constant [41]. In this calculation, the calculated value of the effective Richardson constant for AlInGaN was 25 A cm^{–2} K^{–2}, based on the effective electron masses *m** = 0.22*m*₀ for GaN, *m** = 0.11*m*₀ for InN, and

*m** = 0.40*m*₀ for AlN [39]. The value of the barrier height is calculated to be 0.46 eV for the straightforward diode. The ideality factor *n* of the diode can be obtained from the slope of the linear region in the forward bias, and it was given by the equation below,

$$n = \frac{q}{kT} \left[\frac{dV}{d\ln(I)} \right] \tag{4}$$

The value of ideality factor for our p–n junction was calculated to be 10.6 at the room temperature. Al/p–Si/n–GaN/Ag diode designed by Yakuphanouglu et al. was deposited by a Vaksis thermal evaporation system. After the current–voltage measurement under dark [42]. It was found that the turn-on voltage and breakdown voltage located at about 0.3 and –0.4 V, respectively. Compared with the model for the III-nitride based p–n junction diode, our Al/n–AlInGaN/p–Si/Pt diode has a substantial increase in the breakdown voltage. Similar to this work, the performance of the n-InGaN/p–Si diode was reported by Tuan et al. [26]. The barrier heights of the In_xGa_{1–x}N based diodes decreased from 0.60, 0.56 to 0.53 eV and the ideality factors of the diodes decreased from 6.2, 5.2 to 4.3 with the increase in the indium contents from 0, 0.15, to 0.40, respectively. As is mentioned in C. C. Li’s publication, the sputtered InGaN films with high indium content show the improved crystal quality [24]. Thus the diode containing a richer indium content has a lower intensity of defects or impurities and a lower ideality factor. Caused by the Al incorporation into the InGaN system which behaves higher crystal quality than one of the quaternary system, the sputtered n-AlInGaN/p–Si diode shows the high value of ideality factor and small barrier height. From the measured I–V curve and the calculated data for the n-AlInGaN/p–Si diode, the sputtered AlInGaN film has shown its prospects for the application in electronic devices in a cost-effective way.

In this study, AlInGaN films deposited at 200 °C from a series of targets containing a constant of 25 % In but a variety of Al compositions have been successfully demonstrated. It has been difficult for the aluminum to incorporate into InGaN films by MOCVD in such low deposited temperature. Though Shinoda and Mutsukura [43] had AlGaIn films by sputtering with the (Al + Ga) target at 600–850 °C, the aluminum content failed to dissolve into GaN and the Ga-containing alloy targets behaved viscously while sputtering temperature was below 600 °C. However, our group aims to figure out a solution to alloy aluminum into III-nitride films by reactive sputtering technique at a much lower temperature. In our preliminary attempts for alloying the aluminum into the GaN film by sputtering at and below 400 °C, the obtained AlGaIn film behaved as an insulator, indicating the AlN precipitation around grain boundary to block the current flow. At the low

deposition temperature, the Al atoms bombarded from the target were not gained enough energy to dissolve into the Ga lattice site and to form the AlGa₂N semiconductor. In this work, we demonstrate the feasibility of the Al content alloying into GaN with the assistance of In. With the increasing Al contents of the AlInGa₂N films obtained from target A, B, and C, the 25 % indium added in the targets has improved the incorporation of Al into the InGa₂N films. Our basic AlInGa₂N/Si diode has been fabricated to demonstrate the potential of our sputtered AlInGa₂N for the application of the electronic devices.

4 Conclusion

Crystalline AlInGa₂N films have been deposited on the Si substrates with the magnetron RF reactive sputtering technique. Good adhesion between AlInGa₂N film and Si substrate was observed. The AlInGa₂N film surface was smooth with roughness values of 2.17–2.51 nm. Al incorporated into the InGa₂N films with composition ratios of 1.81, 2.10, and 5.23 % for films from the targets containing Al contents of 5, 7.5, and 15 %, respectively. The enhanced mobility and decreased carrier concentration of the film indicate the successful incorporation of the Al into the lattice site of AlInGa₂N alloy system. The Al alloying in films leads to the preferred growth orientation of the (10 $\bar{1}$ 0) facet. The optical properties of the AlInGa₂N alloy system are strongly affected by Al and In contents or the [Al]/[In] ratio. The decrease in optical bandgap value of AlInGa₂N to the visible region occurs for films with a lower [Al]/[In] ratio. The sputtered AlInGa₂N film able to form a simple n-AlInGa₂N/p-Si junction diode with the turn-on voltage of 2.70 V can have the further potential application in the electron device.

References

1. B. Monemar, G. Pozina, *Prog. Quantum Electron.* **24**, 239–290 (2000)
2. F. Berthet, Y. Guhel, H. Gualous, B. Boudart, J.-L. Trolet, M. Piccione, V. Sbrugnera, B. Grimbart, C. Gaquière, *Solid State Electron.* **72**, 15–21 (2012)
3. I. Saidi, Y. Cordier, M. Chmielowska, H. Mejri, H. Maaref, *Solid State Electron.* **61**, 1–6 (2011)
4. Z. Alaie, S. Mohammad Nejad, M.H. Yousefi, *Mater. Sci. Semicond. Process.* **29**, 16–55 (2015)
5. X. Wang, A. Yoshikawa, *Prog. Cryst. Growth Charact. Mater.* **48–49**, 42–103 (2004)
6. F. Yam, K.Z. Hassan, *Superlattice Microstruct.* **43**, 1–23 (2008)
7. T. Matsuoka, N. Yoshimoto, T. Sasaki, A. Katsui, *J. Electron. Mater.* **21**, 157–163 (1992)
8. F. McIntosh, K. Boutros, J. Roberts, S. Bedair, E. Piner, N. El-Masry, *Appl. Phys. Lett.* **68**, 40–42 (1996)
9. J. Han, A.V. Nurmikko, *IEEE J. Sel. Top. Quantum Electron.* **8**, 289–297 (2002)
10. J. Li, K.B. Nam, K.H. Kim, J.Y. Lin, H.X. Jiang, *Appl. Phys. Lett.* **78**, 61–63 (2001)
11. M.E. Aumer, S.F. LeBoeuf, F.G. McIntosh, S.M. Bedair, *Appl. Phys. Lett.* **75**, 3315–3317 (1999)
12. J.P. Liu, B.S. Zhang, M. Wu, D.B. Li, J.C. Zhang, R.Q. Jin, J.J. Zhu, J. Chen, J.F. Wang, Y.T. Wang, H. Yang, *J. Cryst. Growth* **260**, 388–393 (2004)
13. R. Loganathan, K. Prabakaran, S. Pradeep, S. Surender, S. Singh, K. Baskar, *J. Alloys Compd.* **656**, 640–646 (2016)
14. S.F. Yu, S.J. Chang, R.M. Lin, Y.H. Lin, Y.C. Lu, S.P. Chang, Y.Z.S.P. Chiou, *J. Cryst. Growth* **312**, 1920–1924 (2010)
15. B.Z. Wang, X.L. Wang, *J. Inorg. Mater.* **24**, 559–562 (2009)
16. M.A. Abid, H. Abu Hassan, Z. Hassan, S.S. Ng, S.K. Mohd Bakhori, N.H.A. Raof, *Mater. Sci. Semicond. Process.* **14**, 164–169 (2011)
17. J. Kim, B.K. Kang, S.N. Lee, J. Choi, K.M. Song, *Curr. Appl. Phys.* (2015). doi:10.1016/j.cap.2015.10.017
18. T. Liu, S.J. Jiao, D.B. Wang, L.C. Zhao, T.P. Yang, Z.G. Xiao, *Appl. Surf. Sci.* **301**, 178–182 (2014)
19. S. Suihkonen, O. Svensk, P.T. Torma, M. Ali, M. Sopanen, H. Lipsanen, M.A. Odnoblyudo, V.E. Bougrov, *J. Cryst. Growth* **310**, 1777–1780 (2008)
20. J.W. Shon, J. Ohta, K. Ueno, A. Kobayashi, H. Fujioka, *Sci. Rep.* **4**, 1–4 (2014)
21. J.W. Shon, J. Ohta, K. Ueno, A. Kobayashi, H. Fujioka, *Appl. Phys. Express* **7**, 085502 (2014)
22. E. Nakamura, K. Ueno, J. Ohta, H. Fujioka, M. Oshima, *Appl. Phys. Lett.* **104**, 051121 (2014)
23. C.C. Li, D.H. Kuo, *J. Mater. Sci. Mater. Electron.* **25**, 1404–1409 (2014)
24. C.C. Li, D.H. Kuo, P.W. Hsieh, Y.-S. Huang, *J. Electron. Mater.* **42**, 2445–2449 (2013)
25. C.C. Li, D.H. Kuo, *J. Mater. Sci. Mater. Electron.* **25**, 1942–1948 (2014)
26. T.T.A. Tuan, D.H. Kuo, K. Lin, G.Z. Li, *Thin Solid Films* **589**, 182–187 (2015)
27. D.H. Kuo, T.T.A. Tuan, C.C. Li, W.C. Yen, *Mater. Sci. Eng. B* **193**, 13–19 (2015)
28. Y.K. Fu, Y.H. Lu, R.H. Jiang, B.C. Chen, Y.H. Fang, R. Xuan, Y.K. Su, C.F. Lin, J.F. Chen, *Solid State Electron.* **62**, 142–145 (2011)
29. S.Y. Hu, Y.C. Lee, Y.H. Weng, I.T. Ferguson, Z.C. Feng, *J. Alloys Compd.* **587**, 153–157 (2014)
30. J.P. Ahl, J. Hertkorn, H. Koch, B. Galler, B. Michel, M. Binder, B. Holländer, *J. Cryst. Growth* **398**, 33–39 (2014)
31. I. Ansara, J.P. Bros, C. Girard, *Calphad* **2**, 187–196 (1978)
32. C.B. Soh, W. Liu, S.J. Chua, S. Tripathy, D.Z. Chi, *J. Cryst. Growth* **268**, 478–483 (2004)
33. Y. Liu, T. Egawa, H. Ishikawa, T. Jimbo, *J. Cryst. Growth* **259**, 245–251 (2003)
34. Y. Li, J. Zhang, W. Wan, Y. Zhang, Y. Nie, J. Zhang, Y. Hao, *Phys. E* **67**, 77–83 (2015)
35. S.Y. Hu, Y.C. Lee, Z.C. Feng, S.H. Yang, *J. Lumin.* **132**, 1037–1040 (2012)
36. T.C. Wang, H.C. Kuo, Z.H. Lee, C.C. Chuo, M.Y. Tsai, C.E. Tsai, T.D. Lee, T.C. Lu, J. Chi, *J. Cryst. Growth* **287**, 582–585 (2006)
37. H. Hirayama, A. Kinoshita, T. Yamabi, Y. Enomoto, A. Hirata, T. Araki, Y. Nanishi, Y. Aoyagi, *Appl. Phys. Lett.* **80**, 207–209 (2002)
38. J.P. Liu, G.D. Shen, J.J. Zhu, S.M. Zhang, D.S. Jiang, H. Yang, *J. Cryst. Growth* **295**, 7–11 (2006)

39. A.J. Ghazai, H. Abu Hassan, Z. Hassan, A.S. Hussein, Optoelectron. Adv. Mater. Rapid Commun. **6**, 324–326 (2012)
40. D.K. Schroder, *Semiconductor Material and Device Characterization* (Wiley-Interscience, Hoboken, 2006)
41. S.M. Sze, *Physics of Semiconductor Devices* (Wiley, New York, 1981)
42. F. Yakuphanoglu, F.S. Shokr, R.K. Gupta, A.A. Al-Ghamdi, S. Bin-Omran, Y. Al-Turki, F. El-Tantawy, J. Alloys Compd. **650**, 671–675 (2015)
43. H. Shinoda, N. Mutsukura, Thin Solid Films **516**, 2837–2842 (2008)